INTERNATIONAL JOURNAL FOR NUMERICAL METHODS IN FLUIDS
Int. J. Numer. Meth. Fluids 2010; **62**:313–326
Published online 13 March 2009 in Wiley InterScience (www.interscience.wiley.com). DOI: 10.1002/fld.2026

Shortcomings of discontinuous-pressure finite element methods on a class of transient problems

C. S. Jog*, † and Rakesh Kumar

Department of Mechanical Engineering, Indian Institute of Science, Bangalore 560012, India

SUMMARY

Past studies that have compared LBB stable discontinuous- and continuous-pressure finite element formulations on a variety of problems have concluded that both methods yield solutions of comparable accuracy, and that the choice of interpolation is dictated by which of the two is more efficient. In this work, we show that using discontinuous-pressure interpolations can yield inaccurate solutions at large times on a class of transient problems, while the continuous-pressure formulation yields solutions that are in good agreement with the analytical solution. Copyright © 2009 John Wiley & Sons, Ltd.

Received 7 July 2008; Revised 3 February 2009; Accepted 4 February 2009

KEY WORDS: finite; element; incompressible flow; viscous flow; laminar flow; Navier Stokes

1. INTRODUCTION

In discontinuous-pressure finite elements, typically implemented using a penalty approach, the pressure variable can be eliminated at an element level, and only the velocity degrees of freedom need to be solved for, resulting in an increase in efficiency of the resulting numerical scheme. Hence, this method has been used extensively for the analysis of incompressible fluid flows [1–12], and is even used in commercial finite element codes. Kim and Decker [10] compared solutions obtained using continuous-pressure formulations (which we will subsequently refer to as velocity–pressure formulations) and discontinuous-pressure formulations (which we will subsequently refer to as penalty formulations) implemented using a consistent penalty finite element approach [8], and concluded that both formulations yielded solutions of comparable accuracy, with the penalty formulation being more computationally efficient due to the implicit treatment of the pressure field. Similar conclusions have been drawn by other authors as well. The only disadvantage of the penalty method mentioned in the literature is regarding the choice of the penalty term—a low

*Correspondence to: C. S. Jog, Department of Mechanical Engineering, Indian Institute of Science, Bangalore 560012, India.
†E-mail: jogc@mecheng.iisc.ernet.in

penalty parameter value leads to an inaccurate satisfaction of the mass-conservation equation, while a high value leads to numerical ill-conditioning.

We show in this work that the although the discontinuous-pressure finite element method does lead to accurate solutions in most situations, it can lead to inaccurate solutions on a class of transient problems. We emphasize that the problem is due to the discontinuous-pressure field and not due to an improper choice of penalty parameter, since an independent direct implementation of the discontinuous-pressure approach, where we simultaneously solve for the velocity and pressure as global variables *without* using the penalty method, yielded almost identical results as those obtained using the penalty method.

For the sake of completeness and also since so many different implementations of both methods are possible, in Section 2, we shall briefly describe our formulation and implementation of the consistent penalty and velocity–pressure finite element formulations. We use a 'tangent stiffness' matrix for both the formulations (Kim and Decker [10] use a 'secant' stiffness in their consistent penalty finite element formulation—note that using a tangent stiffness is crucial to obtain a quadratic rate of convergence in the vicinity of the solution). In Section 3, we first present problems where both the discontinuous and continuous-pressure formulations yield good results, and then present the class of transient problems where the discontinuous-pressure formulation fails to yield a correct solution. In Section 4, we draw the conclusions from this study.

2. FORMULATION

Let Ω denote the domain whose boundary Γ is composed of two regions, Γ_u and Γ_t. We are interested in finding an approximate numerical solution to the following initial-boundary value problem.

Find the velocities $\mathbf{u}$, stresses $\boldsymbol{\tau}$, rate of deformation $\mathbf{D}$, and tractions $\mathbf{t}$, such that

$$\nabla\cdot\mathbf{u}=0 \quad \text{on } \Omega \tag{1}$$

$$\rho\left[\frac{\partial\mathbf{u}}{\partial t}+(\nabla\mathbf{u})\mathbf{u}\right]=\nabla\cdot\boldsymbol{\tau}+\rho\mathbf{b} \quad \text{on } \Omega \tag{2}$$

$$\boldsymbol{\tau}=-p\mathbf{I}+2\mu\mathbf{D} \quad \text{on } \Omega \tag{3}$$

$$\mathbf{D}=\tfrac{1}{2}[(\nabla\mathbf{u})+(\nabla\mathbf{u})^{\mathrm{T}}] \quad \text{on } \Omega \tag{4}$$

$$\mathbf{t}=\boldsymbol{\tau}\mathbf{n} \quad \text{on } \Gamma \tag{5}$$

$$\mathbf{t}=\bar{\mathbf{t}} \quad \text{on } \Gamma_t \tag{6}$$

$$\mathbf{u}=\bar{\mathbf{u}} \quad \text{on } \Gamma_u \tag{7}$$

$$\mathbf{u}(0)=\mathbf{u}_0 \quad \text{on } \Omega \tag{8}$$

where $\nabla\mathbf{u}$ denotes the gradient of the velocity, p is the pressure, μ is the dynamic viscosity coefficient, $\mathbf{n}$ is the outward normal to Γ, $\mathbf{b}$ is the prescribed body force on Ω, $\bar{\mathbf{t}}$ and $\bar{\mathbf{u}}$ are the prescribed tractions and velocities on Γ_t and Γ_u, respectively, and $\mathbf{u}_0$ is the initial velocity prescribed on the domain. Note that Γ_t and Γ_u need not be physically disjoint regions. In the penalty and velocity–pressure formulations described below, for every degree of freedom, we require that

DOI: 10.1002/fld

either the tractions or the velocities be prescribed on the boundary. Thus, for example, at a point on the boundary, the traction component t_x and the velocity components (u_y, u_z) could be prescribed.

In the penalty method, Equation (1) is replaced by the weaker requirement [1–10]

$$p = -\lambda(\nabla \cdot \mathbf{u}) \tag{9}$$

where λ is a user-specified penalty parameter. Thus, the constitutive relation given by Equation (3), now reads

$$\boldsymbol{\tau} = -p\mathbf{I} + \boldsymbol{\sigma} = -p\mathbf{I} + \mathbb{C}\mathbf{D}$$

where $\boldsymbol{\sigma}$ is the viscous stress and $\mathbb{C}$ is the fourth-order constitutive tensor for the viscous stress.

2.1. *Consistent penalty finite element formulation*

The consistent penalty finite element formulation is obtained by enforcing Equations (2), (6), and (9) in a weak sense, and using an independent interpolation for the pressure. Thus, if $(\mathbf{u}_\delta, p_\delta)$ denote the variations of the velocity and pressure fields, respectively, then the weak enforcement of Equation (9) yields

$$\int_\Omega p_\delta \left[\frac{p}{\lambda} + \nabla \cdot \mathbf{u}\right] \mathrm{d}\Omega = 0 \quad \forall p_\delta \tag{10}$$

whereas that of Equations (2) and (6) yield

$$\int_\Omega \mathbf{u}_\delta \cdot \left[\rho \frac{\partial \mathbf{u}}{\partial t} + \rho(\nabla \mathbf{u})\mathbf{u} - \nabla \cdot \boldsymbol{\tau} - \rho\mathbf{b}\right] \mathrm{d}\Omega + \int_{\Gamma_t} \mathbf{u}_\delta \cdot (\mathbf{t} - \bar{\mathbf{t}})\, \mathrm{d}\Gamma = 0 \quad \forall \mathbf{u}_\delta$$

By using the identity $\nabla \cdot (\boldsymbol{\tau}^{\mathrm{T}} \mathbf{u}_\delta) = \mathbf{u}_\delta \cdot (\nabla \cdot \boldsymbol{\tau}) + \nabla \mathbf{u}_\delta : \boldsymbol{\tau}$, the relation $\boldsymbol{\tau} = -p\mathbf{I} + 2\mu\mathbf{D}$, and the divergence theorem, the above equation simplifies to

$$\begin{aligned} &\int_\Omega \rho \mathbf{u}_\delta^{\mathrm{T}} \left[\frac{\partial \mathbf{u}}{\partial t} + (\nabla \mathbf{u})\mathbf{u}\right] \mathrm{d}\Omega - \int_\Omega (\nabla \cdot \mathbf{u}_\delta)\, p\, \mathrm{d}\Omega + \int_\Omega [\mathbf{D}_c(\mathbf{u}_\delta)]^{\mathrm{T}} \mathbb{C}_c \mathbf{D}_c\, \mathrm{d}\Omega \\ &\quad = \int_\Omega \rho \mathbf{u}_\delta^{\mathrm{T}} \mathbf{b}\, \mathrm{d}\Omega + \int_{\Gamma_t} \mathbf{u}_\delta^{\mathrm{T}} \bar{\mathbf{t}}\, \mathrm{d}\Gamma \quad \forall \mathbf{u}_\delta \end{aligned} \tag{11}$$

where $\mathbf{D}_c$ and $\mathbb{C}_c$ denote the rate of deformation and the material constitutive tensor (for the viscous stress) expressed in 'engineering' form as

$$\mathbf{D}_c = \begin{bmatrix} D_{xx} \\ D_{yy} \\ D_{zz} \\ 2D_{xy} \\ 2D_{yz} \\ 2D_{xz} \end{bmatrix}, \quad \mathbb{C}_c = \begin{bmatrix} 2\mu & 0 & 0 & 0 & 0 & 0 \\ 0 & 2\mu & 0 & 0 & 0 & 0 \\ 0 & 0 & 2\mu & 0 & 0 & 0 \\ 0 & 0 & 0 & \mu & 0 & 0 \\ 0 & 0 & 0 & 0 & \mu & 0 \\ 0 & 0 & 0 & 0 & 0 & \mu \end{bmatrix}$$

DOI: 10.1002/fld

Let the velocity and pressure fields, and their variations (denoted by subscript δ) and increments (denoted by subscript Δ), be interpolated as

$$\mathbf{u}=\mathbf{N}\hat{\mathbf{u}}, \quad p=\mathbf{P}\boldsymbol{\beta}$$

$$\mathbf{u}_\delta=\mathbf{N}\hat{\mathbf{u}}_\delta, \quad p_\delta=\mathbf{P}\boldsymbol{\beta}_\delta$$

$$\mathbf{u}_\Delta=\mathbf{N}\hat{\mathbf{u}}_\Delta, \quad p_\Delta=\mathbf{P}\boldsymbol{\beta}_\Delta$$

The shape functions $\mathbf{N}$ are the standard velocity shape functions used in a single-field isoparametric formulation. In order to satisfy the LBB stability conditions [9, 13], pressure interpolations of the form $\beta_0+\beta_1 x+\beta_2 y+\beta_3 z$ (i.e. $\mathbf{P}=[1 \;\; x \;\; y \;\; z]$) and $\beta_0+\beta_1 r+\beta_2 z$ (i.e. $\mathbf{P}=[1 \;\; r \;\; z]$) are used for the 27-node hexahedral and 9-node axisymmetric elements used in this work.

Using the above interpolations, for the 27-node hexahedral element, we have

$$\mathbf{D}_c(\mathbf{u}_\Delta^{k+1})=\mathbf{B}\hat{\mathbf{u}}_\Delta^{k+1}$$

$$(\nabla\mathbf{u}_\Delta^{k+1})\mathbf{u}^k=\mathbf{R}\mathbf{B}_{NL}\hat{\mathbf{u}}_\Delta^{k+1}$$

$$\nabla\cdot\mathbf{u}_\Delta=\mathbf{B}_p\hat{\mathbf{u}}_\Delta$$

where

$$\mathbf{B}=\begin{bmatrix} N_{1,x} & 0 & 0 & N_{2,x} & 0 & 0 & . & . & . \\ 0 & N_{1,y} & 0 & 0 & N_{2,y} & 0 & . & . & . \\ 0 & 0 & N_{1,z} & 0 & 0 & N_{2,z} & . & . & . \\ N_{1,y} & N_{1,x} & 0 & N_{2,y} & N_{2,x} & 0 & . & . & . \\ 0 & N_{1,z} & N_{1,y} & 0 & N_{2,z} & N_{2,y} & . & . & . \\ N_{1,z} & 0 & N_{1,x} & N_{2,z} & 0 & N_{2,x} & . & . & . \end{bmatrix}$$

$$\mathbf{B}_p=[N_{1,x} \;\; N_{1,y} \;\; N_{1,z} \;\; N_{2,x} \;\; N_{2,y} \;\; N_{2,z} \;\; . \;\; . \;\; .]$$

$$\mathbf{R}=\begin{bmatrix} u_x^k & u_y^k & u_z^k & 0 & 0 & 0 & 0 & 0 & 0 \\ 0 & 0 & 0 & u_x^k & u_y^k & u_z^k & 0 & 0 & 0 \\ 0 & 0 & 0 & 0 & 0 & 0 & u_x^k & u_y^k & u_z^k \end{bmatrix}$$

$$\mathbf{B}_{NL}=\begin{bmatrix} N_{1,x} & 0 & 0 & N_{2,x} & 0 & 0 & . & . & . \\ N_{1,y} & 0 & 0 & N_{2,y} & 0 & 0 & . & . & . \\ N_{1,z} & 0 & 0 & N_{2,z} & 0 & 0 & . & . & . \\ 0 & N_{1,x} & 0 & 0 & N_{2,x} & 0 & . & . & . \\ 0 & N_{1,y} & 0 & 0 & N_{2,y} & 0 & . & . & . \\ 0 & N_{1,z} & 0 & 0 & N_{2,z} & 0 & . & . & . \\ 0 & 0 & N_{1,x} & 0 & 0 & N_{2,x} & . & . & . \\ 0 & 0 & N_{1,y} & 0 & 0 & N_{2,y} & . & . & . \\ 0 & 0 & N_{1,z} & 0 & 0 & N_{2,z} & . & . & . \end{bmatrix}$$

DOI: 10.1002/fld

Let

$$\mathbf{M}=\int_{\Omega}\rho\mathbf{N}^{\mathrm{T}}\mathbf{N}\,\mathrm{d}\Omega$$

$$\mathbf{G}=\int_{\Omega}\mathbf{P}^{\mathrm{T}}\mathbf{B}_{p}\,\mathrm{d}\Omega$$

$$\mathbf{H}=\int_{\Omega}\frac{1}{\lambda}\mathbf{P}^{\mathrm{T}}\mathbf{P}\,\mathrm{d}\Omega$$

$$\mathbf{Q}=\int_{\Omega}\rho\mathbf{N}^{\mathrm{T}}[(\nabla\mathbf{u}^{k})\mathbf{N}+\mathbf{R}\mathbf{B}_{NL}]\,\mathrm{d}\Omega+\int_{\Omega}\mathbf{B}^{\mathrm{T}}\mathbb{C}_{c}\mathbf{B}\,\mathrm{d}\Omega$$

$$\mathbf{K}^{k}=\mathbf{Q}+\mathbf{G}^{\mathrm{T}}\mathbf{H}^{-1}\mathbf{G}$$

$$\mathbf{f}_{1}=\int_{\Omega}\rho\mathbf{N}^{\mathrm{T}}\mathbf{b}\,\mathrm{d}\Omega+\int_{\Gamma_{t}}\mathbf{N}^{\mathrm{T}}\bar{\mathbf{t}}\,\mathrm{d}\Gamma-\int_{\Omega}[\mathbf{B}^{\mathrm{T}}\boldsymbol{\tau}_{c}^{k}+\rho\mathbf{N}^{\mathrm{T}}(\nabla\mathbf{u}^{k})\mathbf{u}^{k}]\,\mathrm{d}\Omega$$

$$\mathbf{f}_{2}=-\int_{\Omega}\mathbf{P}^{\mathrm{T}}\left[\frac{p^{k}}{\lambda}+\nabla\cdot\mathbf{u}^{k}\right]\mathrm{d}\Omega$$

$$\mathbf{f}_{\Delta}^{k}=\mathbf{f}_{1}+\mathbf{G}^{\mathrm{T}}\mathbf{H}^{-1}\mathbf{f}_{2}$$

Note that since the pressure interpolation is allowed to be discontinuous across element boundaries, $\mathbf{H}^{-1}$ is composed of distinct block matrices $\mathbf{H}_{(e)}^{-1}$ associated with each element. Thus, the element stiffness matrix is given by

$$\mathbf{K}_{(e)}^{k}=\mathbf{Q}_{(e)}+\mathbf{G}_{(e)}^{\mathrm{T}}\mathbf{H}_{(e)}^{-1}\mathbf{G}_{(e)} \tag{12}$$

where the matrices are now formulated over Ω_e, the domain of each element.

Let the previous and current time steps be denoted by the superscripts n and $n+1$, let the superscript k denote the value of that variable at the kth iteration in the $n+1$th time step, and let t_{Δ}^{n+1} denote the difference $t^{n+1}-t^{n}$. By using a generalized trapezoidal rule, where the solution is approximated by

$$\hat{\mathbf{u}}^{t^{n+1}}=\hat{\mathbf{u}}^{t^{n}}+[(1-\alpha)\dot{\hat{\mathbf{u}}}^{t^{n}}+\alpha\dot{\hat{\mathbf{u}}}^{t^{n+1}}]t_{\Delta}^{n+1}$$

the final system of equations is given by

$$(\mathbf{M}+\alpha t_{\Delta}^{n+1}\mathbf{K}^{k})(\hat{\mathbf{u}}_{\Delta}^{k+1})^{t^{n+1}}=t_{\Delta}^{n+1}[(1-\alpha)\mathbf{f}^{t^{n}}+\alpha(\mathbf{f}_{\Delta}^{k})^{t^{n+1}}]+\int_{\Omega}\rho\mathbf{N}^{\mathrm{T}}[\mathbf{u}^{t^{n}}-(\mathbf{u}^{k})^{t^{n+1}}]\,\mathrm{d}\Omega \tag{13}$$

where $\hat{\mathbf{u}}^{0}=\hat{\mathbf{u}}_{0}$ and $\mathbf{f}^{t^{n}}=\int_{\Omega}\rho\mathbf{N}^{\mathrm{T}}\dot{\mathbf{u}}^{t^{n}}$. The steady-state solution (when it exists) can be obtained directly without time-stepping by solving

$$\mathbf{K}^{k}\hat{\mathbf{u}}_{\Delta}^{k+1}=\mathbf{f}_{\Delta}^{k}$$

DOI: 10.1002/fld

2.2. Velocity–pressure integrated formulation

In the velocity–pressure formulation, instead of using Equation (10), we now use

$$\int_\Omega p_\delta \nabla \cdot \mathbf{u}\, \mathrm{d}\Omega = 0 \quad \forall p_\delta \tag{14}$$

In accordance with the LBB conditions, the velocity–pressure interpolations that are used in this work are 27/8-c and 9/4-c for the 27-node hexahedral and 9-node axisymmetric elements, where 'c' denotes a continuous-pressure interpolation. We denote these continuous-pressure interpolation functions by $\mathbf{N}_p$. The semi-discrete equations are now of the form

$$\mathbf{M}\begin{bmatrix} \dot{\hat{\mathbf{u}}}^{k+1} \\ \dot{\hat{\mathbf{p}}}^{k+1} \end{bmatrix} + \mathbf{K}^k \begin{bmatrix} \hat{\mathbf{u}}_\Delta^{k+1} \\ \hat{\mathbf{p}}_\Delta^{k+1} \end{bmatrix} = \mathbf{f}_\Delta^k$$

where with

$$\mathbf{K}_{uu} = \int_\Omega \rho \mathbf{N}^{\mathrm{T}}[(\nabla \mathbf{u}^k)\mathbf{N} + \mathbf{R}\mathbf{B}_{NL}]\, \mathrm{d}\Omega + \int_\Omega \mathbf{B}^{\mathrm{T}} \mathbb{C}_c \mathbf{B}\, \mathrm{d}\Omega$$

$$\mathbf{K}_{up} = -\int_\Omega \mathbf{B}_p^{\mathrm{T}} \mathbf{N}_p\, \mathrm{d}\Omega$$

$$\mathbf{K}_{pu} = \int_\Omega \mathbf{N}_p^{\mathrm{T}} \mathbf{B}_p\, \mathrm{d}\Omega$$

$$\mathbf{K}_{pp} = \mathbf{0}$$

$$\mathbf{f}_1^k = \int_\Omega \rho \mathbf{N}^{\mathrm{T}} \mathbf{b}\, \mathrm{d}\Omega + \int_{\Gamma_t} \mathbf{N}^{\mathrm{T}} \bar{\mathbf{t}}\, \mathrm{d}\Gamma - \int_\Omega [\mathbf{B}^{\mathrm{T}} \boldsymbol{\tau}_c^k + \rho \mathbf{N}^{\mathrm{T}} (\nabla \mathbf{u}^k)\mathbf{u}^k]\, \mathrm{d}\Omega$$

$$\mathbf{f}_2^k = -\int_\Omega \mathbf{N}_p^{\mathrm{T}} (\nabla \cdot \mathbf{u}^k)\, \mathrm{d}\Omega$$

we have

$$\mathbf{M} = \begin{bmatrix} \displaystyle\int_\Omega \rho \mathbf{N}^{\mathrm{T}} \mathbf{N}\, \mathrm{d}\Omega & \mathbf{0} \\ \mathbf{0} & \mathbf{0} \end{bmatrix}$$

$$\mathbf{K}^k = \begin{bmatrix} \mathbf{K}_{uu} & \mathbf{K}_{up} \\ \mathbf{K}_{pu} & \mathbf{K}_{pp} \end{bmatrix} \tag{15}$$

$$\mathbf{f}_\Delta^k = \begin{bmatrix} \mathbf{f}_1^k \\ \mathbf{f}_2^k \end{bmatrix}$$

On using the generalized trapezoidal rule, we get the final system of equations as

$$(\mathbf{M} + \alpha t_\Delta^{n+1} \mathbf{K}^k) \begin{bmatrix} (\hat{\mathbf{u}}_\Delta^{k+1})^{t^{n+1}} \\ (\hat{\mathbf{p}}_\Delta^{k+1})^{t^{n+1}} \end{bmatrix} = \begin{bmatrix} \mathbf{f}_u \\ \mathbf{f}_p \end{bmatrix} \tag{16}$$

DOI: 10.1002/fld

where $\mathbf{M}$ and $\mathbf{K}^k$ are given by Equation (15), and

$$\mathbf{f}_u = t_\Delta^{n+1}[(1-\alpha)\mathbf{f}^{t^n} + \alpha(\mathbf{f}_1^k)^{t^{n+1}}] + \int_\Omega \rho \mathbf{N}^{\mathrm{T}}[\mathbf{u}^{t^n} - (\mathbf{u}^k)^{t^{n+1}}]\,\mathrm{d}\Omega$$

$$\mathbf{f}_p = \alpha t_\Delta^{n+1}(\mathbf{f}_2^k)^{t^{n+1}}\,\mathrm{d}\Omega$$

Updating the viscous stresses corresponding to the prescribed velocity distribution at the beginning of each time step helps to speed up the convergence within that time step.

As evident from Equations (13) and (16), in the penalty formulation, the global equation solving needs to be carried out for the velocity degrees of freedom alone, while with the velocity–pressure formulation, one needs to additionally solve for the nodal pressure degrees of freedom as well (although, because of the mixed formulation being used, they are much fewer in number compared with the velocity degrees of freedom).

If $\mathbf{u} \equiv [u_r \;\; u_z]^{\mathrm{T}}$ and $\boldsymbol{\tau}_c \equiv [\tau_{rr} \;\; \tau_{zz} \;\; \tau_{rz} \;\; \tau_{\theta\theta}]^{\mathrm{T}}$ denote the velocity and stress components in an axisymmetric formulation, then the relevant matrices are

$$\mathbb{C}_c = \begin{bmatrix} 2\mu & 0 & 0 & 0 \\ 0 & 2\mu & 0 & 0 \\ 0 & 0 & \mu & 0 \\ 0 & 0 & 0 & 2\mu \end{bmatrix}$$

$$\mathbf{B} = \begin{bmatrix} N_{1,r} & 0 & N_{2,r} & 0 & . & . & . \\ 0 & N_{1,z} & 0 & N_{2,z} & . & . & . \\ N_{1,z} & N_{1,r} & N_{2,z} & N_{2,r} & . & . & . \\ \dfrac{N_1}{r} & 0 & \dfrac{N_2}{r} & 0 & . & . & . \end{bmatrix}$$

$$\mathbf{R} = \begin{bmatrix} u_r^k & u_z^k & 0 & 0 \\ 0 & 0 & u_r^k & u_z^k \end{bmatrix}$$

$$\mathbf{B}_{NL} = \begin{bmatrix} N_{1,r} & 0 & N_{2,r} & 0 & . & . & . \\ N_{1,z} & 0 & N_{2,z} & 0 & . & . & . \\ 0 & N_{1,r} & 0 & N_{2,r} & . & . & . \\ 0 & N_{1,z} & 0 & N_{2,z} & . & . & . \end{bmatrix}$$

3. NUMERICAL EXAMPLES

The system of equations in both, the consistent penalty and the velocity–pressure, formulations is solved using the WSMP sparse solver [14, 15], and full integration is used to calculate all the

DOI: 10.1002/fld

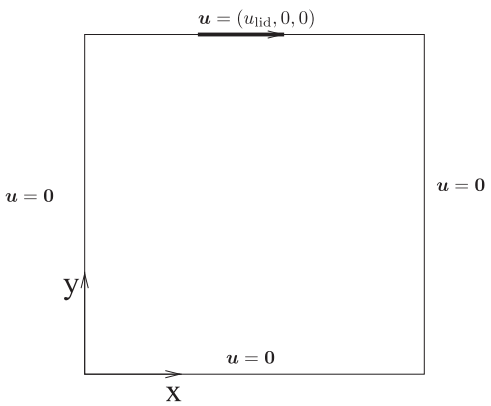

Figure 1. 2-D lid-driven cavity flow.

matrices. We use a value of $\alpha = 1$ (backward Euler) at the first time step, and a value of 0.7 subsequently, in all the examples. In order to validate our implementation, we solved the stick–slip and the abrupt contraction flow problems in Reference [13] (where the Stokes approximation is used). We chose material parameters such that the Stokes approximation is valid. A perfect agreement with the results presented in [13] was obtained.

Jog [16] and Sohn [17] have shown that good results are obtained with the hybrid and consistent penalty methods, respectively, on a variety of steady-state problems (including the 2-D lid-driven cavity problem), and hence, here, we focus only on transient problems. We discuss the transient 2-D lid-driven cavity and bounded oscillatory Stokes flow problems. These examples are deliberately chosen to show that in the first example the penalty method yields a good solution, while in the second one it does not.

3.1. Transient 2-D lid-driven cavity problem

The setup and boundary conditions are as shown in Figure 1. The length and width of the cavity is unity. Since 3-D elements are being used, the z-direction velocity is suppressed for all the nodes, and slip is allowed on the boundary surfaces $z =$ constant so as to mimic a 2-D flow. In order to avoid an 'ill-posed' problem with velocity singularities at the two upper corners, we prescribe the velocity distribution at the upper surface as [18]

$$u_{\mathrm{lid}} = \begin{cases} \tanh(\beta x), & 0 \leqslant x \leqslant 0.5 \\ \tanh(\beta(1-x)), & 0.5 < x \leqslant 1.0 \end{cases}$$

where β is taken to be 50. Note that the above velocity distribution closely emulates the standard singular boundary condition by providing a smooth but sharp transition from $u = 0$ to $u = 1$. The material properties used are $\rho = 400$ and $\mu = 1$ ($Re = 400$), and in the case of the penalty method $\lambda = 10^{10}\mu$. A uniform mesh of $16 \times 16 \times 1$ 27-node hexahedral elements is used to model the

DOI: 10.1002/fld

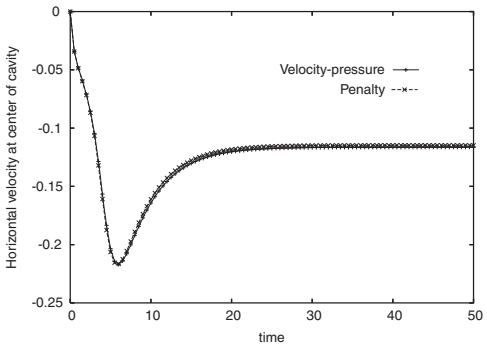

Figure 2. Time history of the horizontal velocity at the center of the cavity.

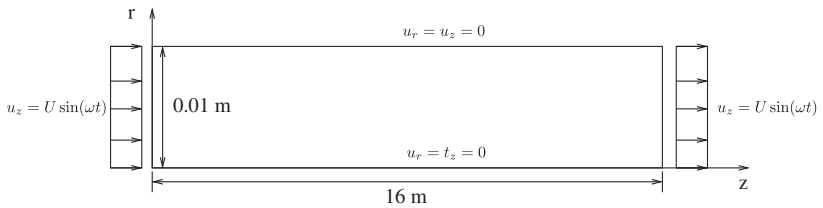

Figure 3. Bounded oscillatory Stokes flow.

domain. The time step used is $t_\Delta = 0.125$. Almost identical results are obtained using the penalty and the velocity–pressure formulations as seen from Figure 2. Moreover, they are also in excellent agreement with the results obtained by Manzari [19] (compare with their Figure 9).

3.2. Bounded oscillatory Stokes flow

The nice feature about this problem is that not only does it have an analytical solution, but it has also been studied experimentally by Akhavan *et al.* [20]. Although the focus of Akhavan *et al.*'s work was on the transition to turbulent flow, here we shall consider only the case of laminar flow in order to allow a comparison with the analytical solution. Another attractive feature of this problem is that since we specify the velocity both at the inlet and outlet, there is no ambiguity associated with boundary conditions. The domain is shown in Figure 3. As in Reference [20], periodic boundary conditions are imposed at the inlet and outlet, and the values used are $U = 0.1107216$ and $\omega = 0.342144$. The 'periodic steady-state' analytical solution derived under the assumption of fully developed flow is given by [21]

$$u(r,t) = 2U\left(1-\frac{r^2}{R^2}\right)\sin\omega t + 4U\omega R^2 \sum_{n=1}^{\infty} \frac{[J_0(\lambda_n r/R) - J_0(\lambda_n)]}{\lambda_n^2 J_0(\lambda_n)[\nu^2\lambda_n^4 + \omega^2 R^4]}[\omega R^2 \sin\omega t + \nu\lambda_n^2 \cos\omega t]$$

DOI: 10.1002/fld

where J_0 is the zero-order Bessel function, λ_n are the positive roots of the second-order Bessel function $J_2(x)$, R is the radius, and v is the kinematic viscosity. The material parameters used are $\rho=1000$, $\mu=0.001$, and in the case of the penalty method, $\lambda=10^{13}\mu$ (almost identical results are obtained with an independent implementation based on Equation (14) instead of Equation (10), where we solve for the velocity and (discontinuous) pressure as global variables *without* using a penalty approach, thus showing that the λ value being used is appropriate).

Uniform coarse and fine meshes of 20×20 and 40×40 axisymmetric elements are used to discretize the domain, and time steps of 0.01 and 0.005, respectively, are used. The coarse and fine mesh results at $z=8$ after 10 cycles[‡] (in order for the flow to reach a periodic steady-state solution) at some instances during the acceleration and deceleration phases are shown in Figures 4 and 5, respectively. Quite remarkably, as seen from the figures, the results of the velocity–pressure formulation are in almost perfect agreement with the analytical solution. In contrast, the penalty formulation results are in error, and at some time instances, there is no reduction in the error even with the use of mesh and time step refinement, e.g. at $\omega t=4\pi/6$ and $\omega t=10\pi/6$, the error at the axis is substantially larger with mesh refinement! We note that the results given by the penalty and velocity–pressure formulations are in close agreement at small times; the errors in the penalty formulation, however, increase progressively with time, resulting in large errors at large times.

Although we have reported the results only for the axisymmetric formulation, similar errors result even with the use of hexahedral penalty finite elements. In addition, although we have reported the penalty formulation errors with one choice of inlet velocity profile, similar errors result with other choices of velocity profile or with different choices of α, in particular $\alpha=0.5$. Furthermore, using a Neumann instead of a Dirichlet boundary condition at the outlet does not reduce the errors in the discontinuous-pressure formulation— the coarse mesh results with such a condition are presented in Figure 6. Thus, it seems that the discontinuous-pressure finite element method yields poor results on the class of axisymmetric bounded oscillatory flows.

Though our purpose in this work is to compare the accuracy of the solutions, we shall briefly also comment on the efficiency of the two schemes. On the 40×40 mesh, the numbers of equations in the penalty and velocity–pressure formulations are 12 561 and 14 241, respectively. Both schemes converge to an unbalanced force norm of less than 10^{-10} in just two iterations within each time step, so that the only difference in cost is due to the difference in the number of equations.

4. CONCLUSIONS

An example of a transient problem presented in this paper shows that notwithstanding the fact that discontinuous-pressure finite element methods work well in a large number of cases, they can be unreliable on a class of bounded oscillatory flow problems where the errors grow with time, and where the solution accuracy does not improve even with mesh and time step refinement. Contrary to the finding in Reference [22], it appears that the LBB conditions may be necessary but not sufficient for stability of solutions in transient problems—a more detailed theoretical analysis needs to be carried out to verify these findings. In spite of its slightly higher cost compared with the penalty method, the continuous-pressure formulation seems to be more robust. The higher

[‡]Thus, e.g. $\omega t=\pi/6$ is actually $\omega t=20\pi+\pi/6$.

DOI: 10.1002/fld

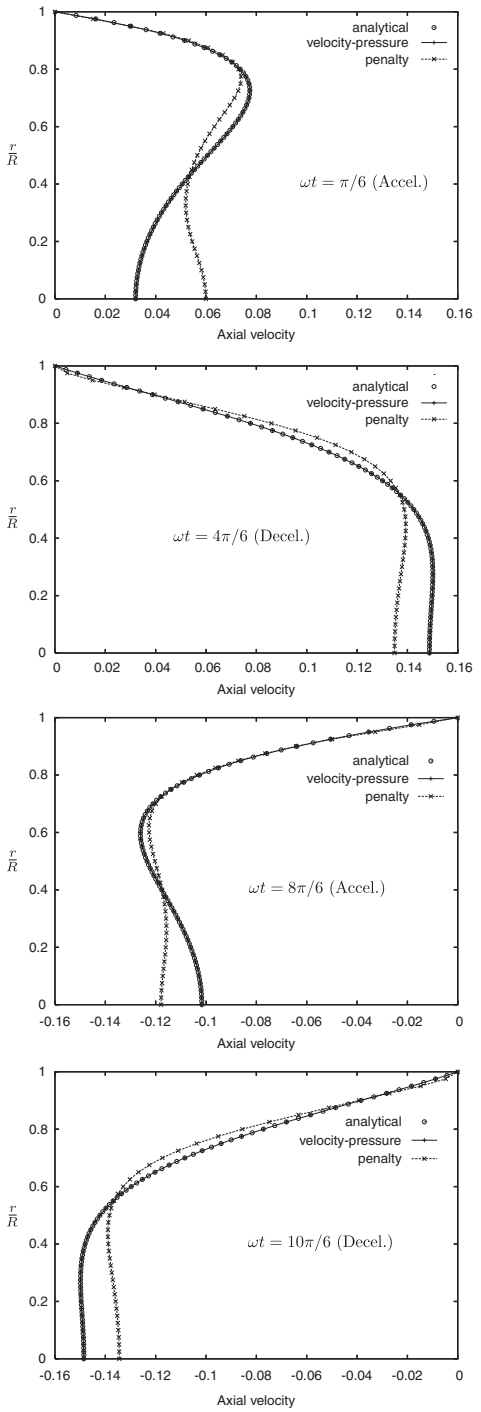

Figure 4. Coarse mesh results for bounded oscillatory Stokes flow.

DOI: 10.1002/fld

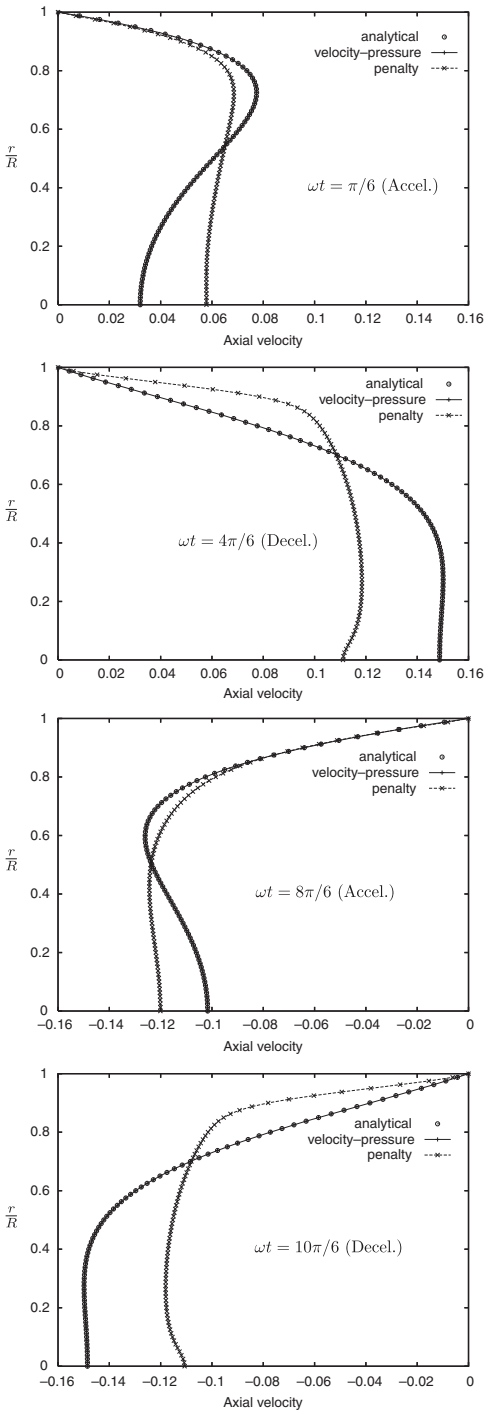

Figure 5. Fine mesh results for bounded oscillatory Stokes flow.

DOI: 10.1002/fld

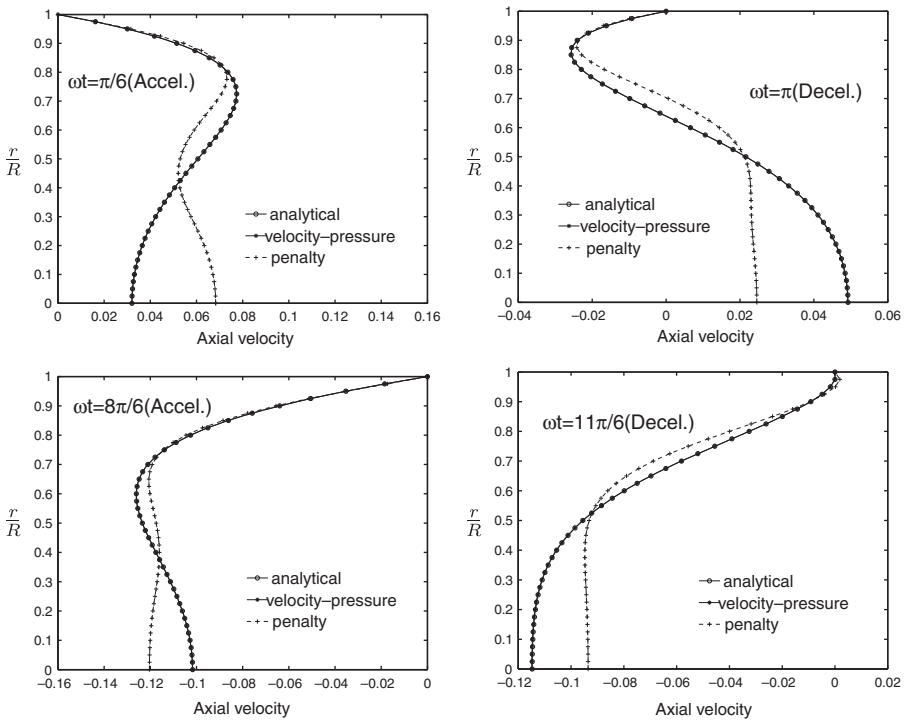

Figure 6. Coarse mesh results for bounded oscillatory Stokes flow with a Neumann boundary condition at the outlet.

cost is also offset by the fact that one directly obtains nodal values of the pressure (which is an important physical variable) without the need for any extrapolation and averaging.

REFERENCES

1. Reddy JN. Penalty-finite-element analysis of 3-D Navier–Stokes equations. *Computer Methods in Applied Mechanics and Engineering* 1982; **35**:87–106.
2. Reddy MP, Reddy JN. Penalty finite element analysis of incompressible flows using element by element solution algorithms. *Computer Methods in Applied Mechanics and Engineering* 1992; **100**:169–205.
3. Reddy MP, Reddy JN. Multigrid methods to accelerate convergence of element-by-element solution algorithms for viscous incompressible flows. *Computer Methods in Applied Mechanics and Engineering* 1996; **132**:179–193.
4. Carey GF, Krishnan R. Penalty finite element method for the Navier–Stokes equations. *Computer Methods in Applied Mechanics and Engineering* 1984; **42**:183–224.
5. Hughes TJR, Liu WK, Brooks A. Finite element analysis of incompressible viscous flows by the penalty function formulation. *Journal of Computational Physics* 1979; **30**:1–60.
6. Bercovier M, Engelman M. A finite element for the numerical solution of viscous incompressible flows. *Journal of Computational Physics* 1979; **30**:181–201.
7. Heinrich JC, Marshall RS. Viscous incompressible flow by a penalty function finite element method. *Computers and Fluids* 1981; **9**:73–83.
8. Engelman MS, Sani RL, Gresho PM, Bercovier M. Consistent vs. reduced integration penalty methods for incompressible media using several old and new elements. *International Journal for Numerical Methods in Fluids* 1982; **2**:25–42.

DOI: 10.1002/fld

9. Dhatt G, Hubert G. A study of penalty elements for incompressible laminar flow. *International Journal for Numerical Methods in Fluids* 1986; **6**:1–19.
10. Kim SW, Decker RA. Velocity–pressure integrated versus penalty finite element methods for high-Reynolds number flows. *International Journal for Numerical Methods in Fluids* 1989; **9**:43–57.
11. Kim SW. A fine grid finite element computation of two-dimensional high-Reynolds number flows. *Computers and Fluids* 1988; **16**:429–444.
12. Gresho PM, Sani RL. *Incompressible Flow and the Finite Element Method*: *Vol. II—Isothermal Laminar Flow*. Wiley: New York, 1998.
13. Ruas V, Carneiro de Araujo JH, Silva Ramos MAM. Multi-field finite element methods with discontinuous pressures for axisymmetric incompressible flows. *Journal of Computational and Applied Mathematics* 2004; **168**:393–402.
14. Gupta A. WSMP: Watson sparse matrix package part II—direct solution of general sparse systems. *IBM Research Report RC 21888* (*98472*), 2000.
15. Gupta A. Recent advances in direct methods for solving unsymmetric sparse systems of linear equations. *ACM Transactions on Mathematical Software* 2002; **28**(3):301–324.
16. Jog CS. A hybrid element formulation for the three-dimensional penalty-finite-element analysis of incompressible fluids. *International Journal for Numerical Methods in Engineering* 2008; **73**:123–145.
17. Sohn JL. Evaluation of FIDAP on some classical laminar and turbulent benchmarks. *International Journal for Numerical Methods in Fluids* 1988; **8**:1469–1490.
18. Pontazza JP, Reddy JN. Space–time coupled spectral/hp least-squared finite element formulation for the incompressible Navier–Stokes equations. *Journal of Computational Physics* 2004; **197**:418–459.
19. Manzari MT. A time-accurate finite element algorithm for incompressible flow problems. *International Journal of Numerical Methods for Heat and Fluid Flow* 2003; **13**(2):158–177.
20. Akhavan R, Kamm RD, Shapiro AH. An investigation of transition to turbulence in bounded oscillatory Stokes flows Part I. Experiments. *Journal of Fluid Mechanics* 1991; **225**:395–422.
21. Jog CS. *Foundations and Applications of Mechanics*: *Vol. II—Fluid Mechanics* (2nd edn). Alpha Science: Oxford, U.K., 2007.
22. Boffi D, Gastaldi L. Analysis of finite element approximation of evolution problems in mixed form. *SIAM Journal on Numerical Analysis* 2004; **42**(4):1502–1526.

DOI: 10.1002/fld